Microstructure Modelling of Silica Bodies from Oil Palm Empty Fruit Bunch (OPEFB) Fibres

Farah Nadia Omar,[a] Mohd Afandi P. Mohammed,[a,*] and Azhari Samsu Baharuddin [a,b]

Investigating the mechanical behaviour of silica bodies in oil palm empty fruit bunches (OPEFB) is important to improve the process of silica body removal. This study will assist in providing an understanding of the role of OPEFB as a bioresource material for the bioconversion process. The microstructure of silica bodies/protrusions on the OPEFB fibre surface was modelled using the finite element method, based on the information obtained from scanning electron microscopy (SEM). The effects of silica body geometry, possible anisotropy/orthotropy, and debonding between the interface of the silica body and OPEFB fibre were investigated. Agreements were observed between the results using both circular and spiked silica body models with different geometries and volume fractions. In addition, the cohesive debonding modelling results showed that once critical stress was activated, the stress-strain curve deviated from the no-debond model. The results also suggested that the value of cohesive energy should be between 0.5 kN/m and 4 kN/m.

Keywords: Oil palm empty fruit bunch; Microstructure modelling; Silica bodies; Cohesive zone modelling

*Contact information: a: Department of Process and Food Engineering, Faculty of Engineering, Universiti Putra Malaysia, 43400 UPM Serdang, Selangor, Malaysia; b: Institute of Tropical Forestry and Forestry Products (INTROP), Putra Infoport, Universiti Putra Malaysia, 43400 UPM, Serdang, Selangor, Malaysia; *Corresponding author: afandi@upm.edu.my*

INTRODUCTION

Oil palm empty fruit bunch (OPEFB) consists of silica bodies embedded in fibre, as shown in Fig. 1(a). Silica bodies are observed in natural fibres such as piassava (d'Almeida *et al.* 2006) and oil palm fruit bunch (Law *et al.* 2007). Investigating the mechanical behaviour of silica bodies in OPEFB is important for several reasons: it will improve the process of silica body removal, so that OPEFB can then be used for biochemical conversion technology (Bahrin *et al.* 2012) and the pulp production industry (Hubbe and Heitmann 2007; Martin-Sampedro *et al.* 2012; Ghazali *et al.* 2009). Additionally, the study will assist in providing an understanding of the role of OPEFB as a bioresource material. One specific application of OPEFB after the silica bodies are removed (using, for example, the stream pretreatment method of Bahrin *et al.* (2012)) is for biocompost, in which the pretreatment firstly removes the silica bodies, followed by depolymerisation of lignin structures, breakage of the cellulose crystalline structure, and finally, an increase in the porosity of the material (Mosier *et al.* 2005). The porosity increase allows better bio-degradation of OPEFB. However, a complete physical understanding of the mechanisms in OPEFB during pretreatment (from silica body removal to degradation of cellulose) would be quite complex; therefore, this study is restricted to the consideration of silica body removal, which is believed to be the first process that occurs in OPEFB due to applied deformation or chemical constraints.

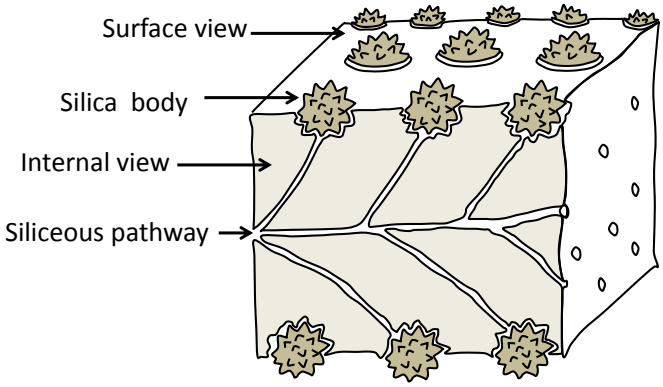

(a)

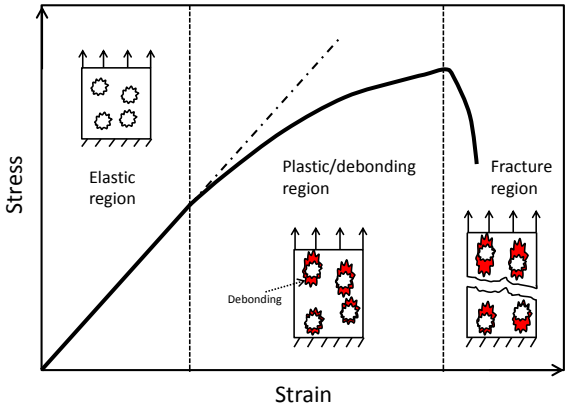

(b)

Fig. 1. (a) Silica bodies embedded in OPEFB fibre (re-drawn from Law *et al.* (2007)), (b) stress-strain curve of OPEFB fibre

There are few studies available in the literature that involve the study of micro-mechanics of silica bodies and OPEFB fibre, as well as their contributions to the mechanical behaviour of OPEFB. In contrast, micromechanical studies on other natural fibres such as wood and plant cell walls are well established (Somerville *et al.* 2004; Burgert 2006; Qi 2009, 2011; Burgert and Dunlop 2011; Hayot *et al.* 2012). It is believed that silica bodies contribute to the strength and rigidity of OPEFB (Nascimento *et al.* 2012). To illustrate this, Fig. 1(b) shows a suggested stress-strain curve of OPEFB, which can be separated into three regions: elastic, plastic/debonding, and fracture.

In the elastic region, the bonding of silica bodies is perfect, and no failure between the interfaces can be observed. In the plastic/debonding region, debonding between the interfaces is believed to cause the curve to deviate from the elastic line (dotted line in Fig. 1(b)). Debonding then continues to accumulate until complete failure occurs in the fracture region. By treating OPEFB as a heterogeneous structure, where the fibre acts as the matrix and silica bodies as fillers, the micromechanical theory of interface debonding of filler and matrix by Meddad and Fisa (1997) can be applied. OPEFB reportedly displays a stress-strain curve similar to Fig. 1(b), as obtained by Yusoff *et al.* (2009) from uniaxial tension tests, who found an elastic region strain limit of ~0.04 and failure strain of ~0.13.

Silica body removal from piassava fibre material is relatively easy; it can be done *via* abrasion, chemical treatment, or mechanical loading (Nascimento *et al.* 2012). However, Bahrin *et al.* (2012) reported that it is difficult to remove silica bodies from OPEFB fibre, as this must be performed using high-pressure steam or chemical treatments. This is in agreement with the results obtained by Yunus *et al.* (2010), where the silica bodies from OPEFB could only be dislodged completely from the OPEFB fibre using a combination of acid hydrolysis at 100 °C and ultrasonic pretreatments. These findings suggest that the behaviour at the interface between silica bodies and OPEFB fibre is important for the removal of silica bodies from OPEFB fibre.

There are a very limited number of publications that have reported on silica body removal mechanisms, as well as the relationship between silica bodies and the fibre components in the OPEFB. As reported in previous works (Currie and Perry 2007; Fang and Ma 2006; Lins *et al.* 2002), silica bodies act as a defensive barrier that protects against bacterial and fungal attacks. It is commonly understood that these biological attacks may only take place when the hydrolase enzymes attach to the exposed amorphous region of the fibre. Therefore, the removal of silica bodies could open up the siliceous pathway and expose more of the amorphous region of the fibres, resulting in better enzymatic hydrolysis performance.

This work therefore investigated the microstructure of silica bodies/protrusions on OPEFB fibre surfaces using scanning electron microscopy (SEM). The information from image analysis results (such as the geometry of the silica bodies and volume fraction) was used in finite element modelling of OPEFB, treating OPEFB as a heterogeneous material. Details of the development of the model in the commercially available finite element software Abaqus (2009) will also be discussed. The investigated parameters include the effect of silica body geometry, possible anisotropy/orthotropy, and debonding between the interface of the silica body and OPEFB fibres. This study will provide an understanding of silica body removal from natural fibres like OPEFB.

MATERIALS AND METHODS

Oil palm empty fruit bunches (OPEFB) were obtained from Besout Palm Oil Mill (Sungkai, Perak, Malaysia; 3°52’59.34’’ N, 101°16’35.87’’ E). The samples were physically pressed to remove oil and moisture before being shredded to sizes between 15 and 20 cm. The shredded samples were then kept in environmentally controlled conditions at -20 °C prior to SEM analysis.

Scanning electron microscopy (SEM) analysis was performed using an electron microscope (S-3400N, Hitachi, Japan). The OPEFB fibres were cut to sizes ranging from 0.2 to 0.5 cm. The samples were then mounted on an aluminium stub using double-sided adhesive tape and were sputter-coated with platinum prior to morphological assessment (E-1010, Hitachi, Japan). The SEM micrographs were obtained with an acceleration voltage of 15 to 25 kV. Images from the SEM analysis of OPEFB fibres are shown in Fig. 2. It was observed that silica bodies (fillers) were embedded in the matrix (OPEFB fibre). The geometry of the fillers was circular with spikes. Similar findings were observed by Law *et al.* (2007) and Bahrin *et al.* (2012). The filler volume fraction was obtained using SEM image analysis in ImageJ software (Rasband 2012). This was performed by converting the image into a binary (black and white) image and calculating the difference between the black and white areas.

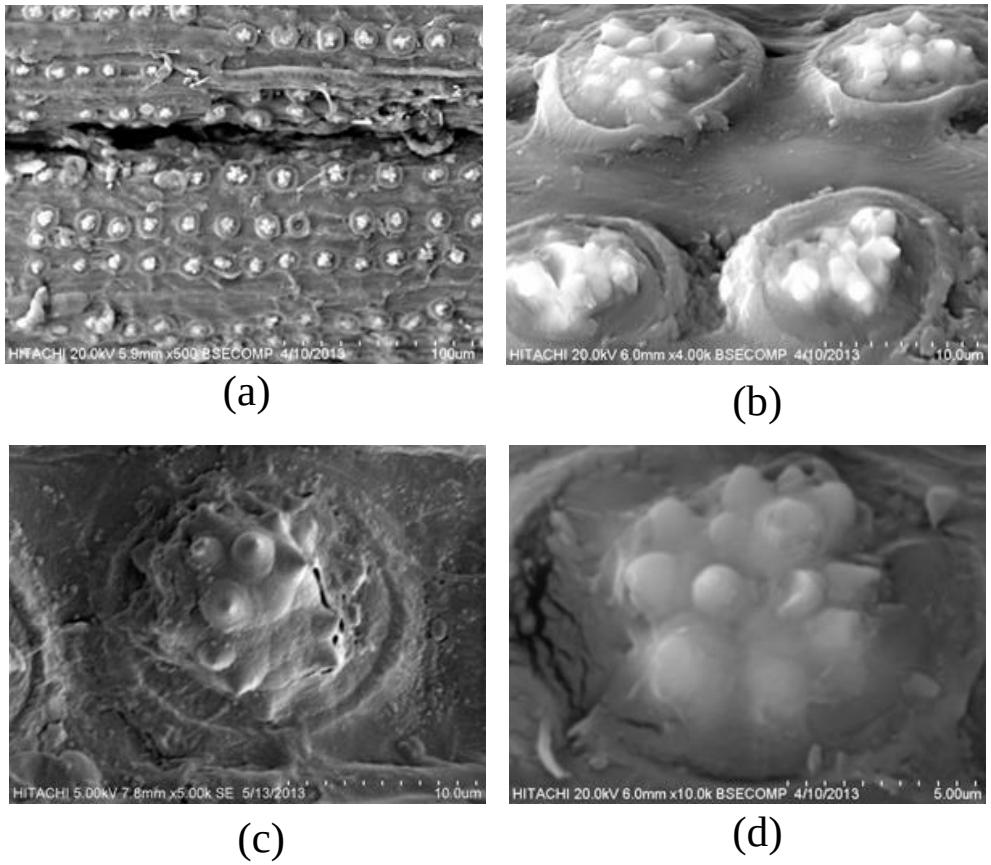

Fig. 2. SEM analysis of silica bodies from OPEFB fibres: (a) 500x magnification, (b) 4000x magnification, (c) 5000x magnification, (d) 10,000x magnification

For OPEFB, volume fraction values of 15% ± 4 were obtained from at least eight SEM images at different magnifications. Note that in this work, it is assumed that the area fraction (obtained from SEM images) is the same as the volume fraction of the fibre, based on the assumption by Underwood (1970). However, an accurate volume fraction (*e.g.* corrected volume fraction) needs to be investigated in the future using a 3D analysis method, since it is possible that the volume fraction is not uniform throughout the cross section of the fibre.

RESULTS AND DISCUSSION

Model Development

OPEFB fibre will be regarded as the matrix and the silica bodies as the filler from this section onward, unless otherwise specified. A 2-D single-particle model of the OPEFB was produced using the commercial finite element software Abaqus with Abaqus/Standard procedure (Abaqus 2009). The single-particle model is presented in Fig. 3(a) and consists of filler embedded in a matrix. The spikes in the filler were produced based on the SEM images shown in the previous section (Fig. 2). The effect of the spikes on the mechanical behaviour of OPEFB will be discussed in detail later in this section. Any sharp edges on the spikes and filler were tapered (see Fig. 3(a)), as sharp edges will affect the convergence of the finite element modelling results.

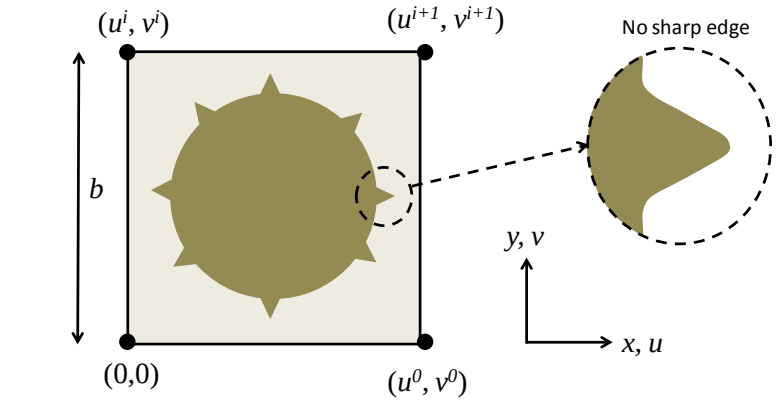

(a)

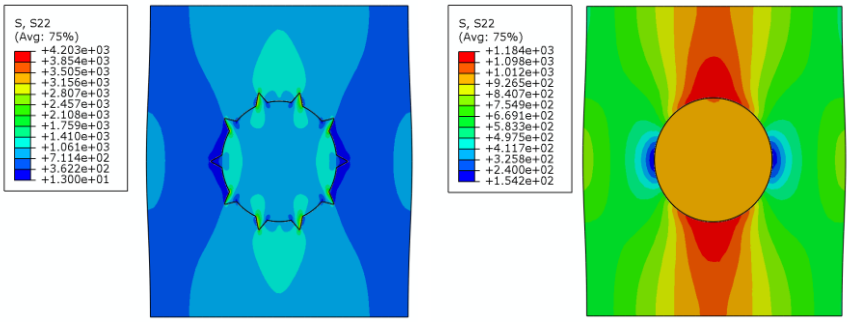

(b) (c)

Fig. 3. (a) The microstructure finite element model of OPEFB and simulation image results of 10-spike filler (b), and circular filler (c) models. The S22 colour scale indicates principal stress in the y direction (values in MPa).

The filler volume fraction for the model was set at 15%, which was obtained from the image analysis performed in the previous section. Plane stress elements (CPS element type) and a 'static' time step were used throughout the analysis. The model was loaded under uniaxial tension, compression, and simple shear modes at a true strain rate of 0.1/s. The following boundary conditions were used for evaluation of uniaxial tension and uniaxial compression:

$$u(0,0) = v(x,0) = 0$$
$$v(x,b) = \delta \quad (1)$$

where δ, the applied displacement, is > 0 under uniaxial tension and < 0 under uniaxial compression; u and v are displacements in the x and y direction, respectively, b is the height of the single-particle model, and (0,0) are the origin coordinates at the lower left

corner of the single particle model (see Fig. 3(a)). Under simple shear, the following boundary conditions were used:

$$u(x,0) = v(x,0) = 0$$
$$u(x,b) = \delta \quad ; \quad v(x,b) = 0 \tag{2}$$

The selection of material for the filler was obtained from d'Almeida *et al.* (2006) and Nordin *et al.* (2013), who reported high traces of silica in the filler based on EDS experiments. Therefore, by assuming the filler is silicon dioxide, a value of 70 GPa was used. The material parameters for the OPEFB were obtained from experimental results by Gunawan *et al.* (2009) as 16 GPa. The elastic moduli of the composite, filler, and matrix are related through the following equation (Mishnaevsky 2007), from the classical Voigt composite rule of mixture:

$$E = (1 - f)E_m + fE_f \tag{3}$$

where E, E_m, and E_f are the elastic moduli of the composite, matrix, and fibre, respectively, and f is the filler volume fraction. Using the values E = 16 GPa and E_f = 70 GPa, as well as a volume fraction of 15%, the matrix elastic modulus was simply calculated as E_m = 6.47 GPa. The filler and matrix Poisson's ratio was assumed to be 0.5 (incompressible material). The interface between filler and matrix was set to be perfectly bonded. The debonding at the interface will be discussed in detail later.

The mesh sensitivity study for the finite element model (*i.e.*, 15% filler volume fraction) was performed by varying the number of elements in the finite element model from coarse (3000 elements) to fine (30,000 elements) to ensure a consistent solution. All of the models performed in Abaqus were in agreement with each other (less than 1% difference), which indicated that there is no variation of stress-strain results with the number of meshed elements in the finite element model.

Effect of Filler Volume Fraction

Volume fractions of 10%, 15%, and 20% were used in the simulation with the model with 10 spikes. These were compared to the model without spikes (circular filler) at similar volume fractions, and the results are shown in Fig. 4 under different loading conditions of uniaxial tension, uniaxial compression, and simple shear. The results of the model with spikes are in agreement with those of the circular filler, which suggests that circular filler can be used to model OPEFB fibre.

Effect of Silica Body Geometry

To investigate the effect of circular filler with occurrence of spikes in OPEFB (as observed in Fig. 2), finite element circular models with different numbers of spikes (5, 10, and 20 spikes) and a similar volume fraction (15%) were produced and simulated. This was compared to a model of circular particles using a similar volume fraction. The results are shown in Fig. 5(a) to Fig. 5(c) under uniaxial tension, uniaxial compression, and simple shear modes.

Similar results were obtained using models with different numbers of spikes and the circular model, which further illustrated the advantage of using a circular filler to model OPEFB fibre. Examples of simulation image results of the circular and 10-spike filler models are shown in Fig. 3(b) and Fig. 3(c).

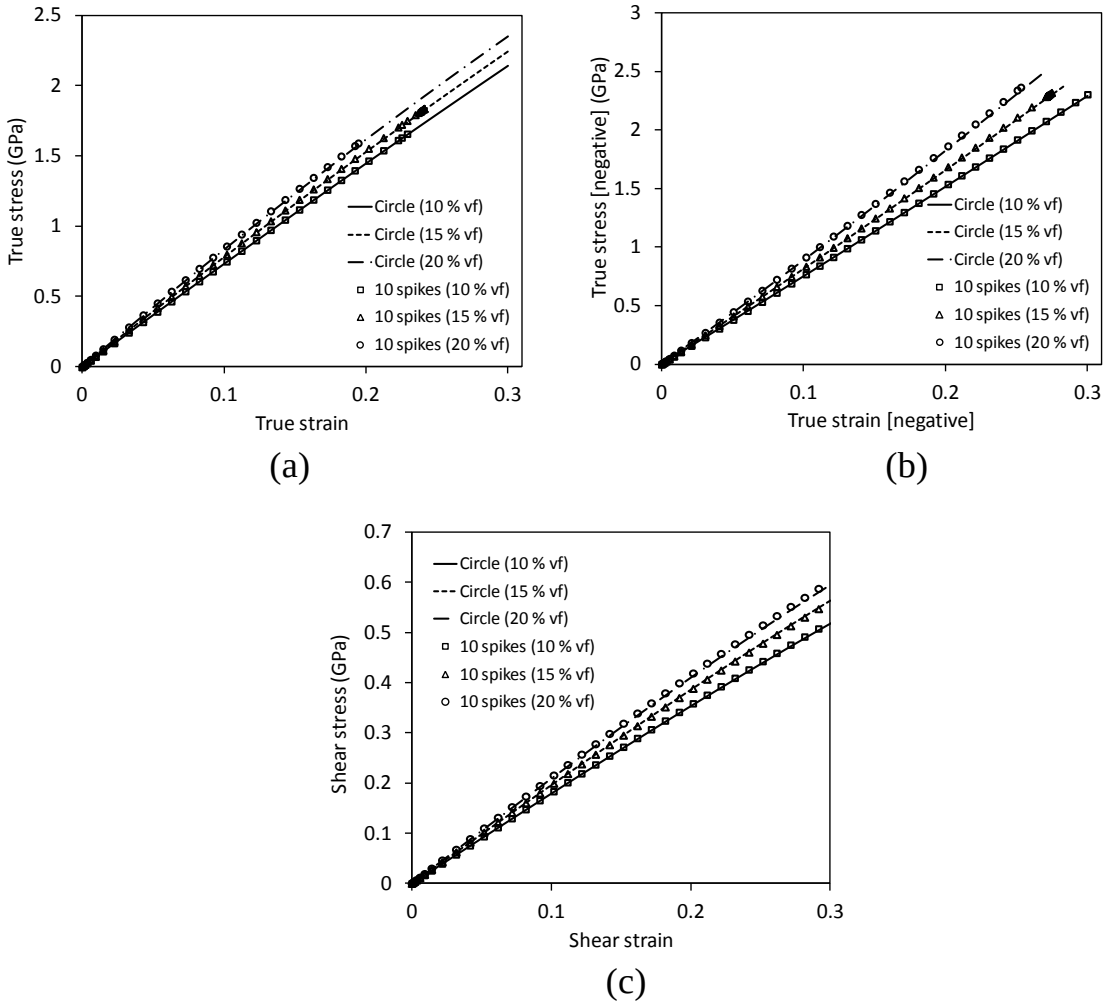

Fig. 4. Effect of filler volume fraction under (a) uniaxial tension, (b) uniaxial compression, and (c) simple shear

Effect of Orthotropy/Anisotropy of OPEFB Matrix

The constitutive model for the matrix in previous sections was assumed to be isotropic and elastic. However, it is possible that anisotropy or orthotropy could be observed in different directions of the matrix. For example, orthotropy in natural fibres (wood-based materials) was reported by Qing and Mishnaevsky (2009, 2011). The SEM image of OPEFB matrix shown in Fig. 2(a) suggests that the fibre is aligned in a longitudinal direction. This indicates the possibility of direction-dependent behaviour for OPEFB (*i.e.*, anisotropy or orthotropy). Because no experimental results have been reported for the anisotropic behaviour of OPEFB, this section provides a numerical investigation of the anisotropy of OPEFB.

For 2-D plane stress elements, the simplified mathematical theory of anisotropy is described as follows (Abaqus 2009):

$$\begin{bmatrix} \sigma_{xx} \\ \sigma_{yy} \\ \tau_{xy} \end{bmatrix} = \begin{bmatrix} E_x & -\nu_{xy}E_x & 0 \\ -\nu_{xy}E_x & E_y & 0 \\ 0 & 0 & G_{xy} \end{bmatrix} \begin{bmatrix} \varepsilon_x \\ \varepsilon_y \\ \gamma_{xy} \end{bmatrix} \quad (4)$$

where σ_{xx} and σ_{yy} are the stresses in the principal directions (see Fig. 3(a) for the principal directions) and τ_{xy} is the shear stress. E_x and E_y are elastic moduli in the principal directions, and G_{xy} and ν_{xy} are the shear modulus and Poisson's ratio, respectively. Finally, the parameters, ε_x and ε_y are the strain in the principal directions, and γ_{xy} is the shear strain. The modelling work in this section was performed as follows: the moduli E_x and ν_{xy} were set to be the same as in previous sections (6.47 GPa and 0.5, respectively). The modulus E_y, on the other hand, was set at half and one quarter the value of E_x (3.235 GPa and 1.617 GPa, respectively). These models were called the anisotropy A and anisotropy B models, respectively. The results are shown in Fig. 5(d), which shows agreement between the models with 10 spikes and those with circular fillers. Lower stress-strain curves were obtained using lower E_y values.

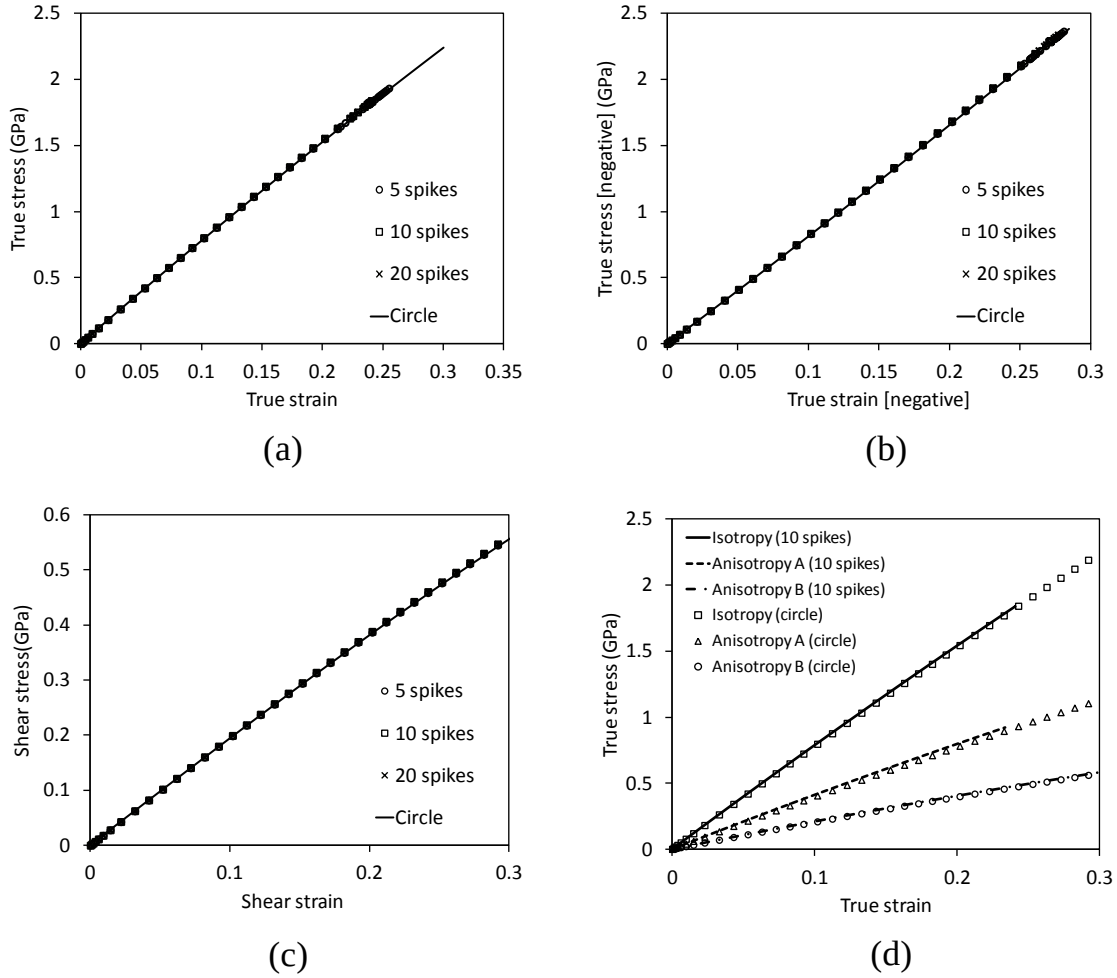

Fig. 5. Effect of silica body geometry under (a) uniaxial tension, (b) uniaxial compression, and (c) simple shear, (d) shows the effect of anisotropy of the single-particle model under uniaxial tension. Note that all the results are shown at 15% filler volume fraction.

Effect of Interface Between Silica Body and Fibre

In this section, cohesive contact was defined between the filler and matrix interface (shown in Fig. 3(a)) to simulate the debonding of the filler (silica bodies) and the matrix (fibre). In the model, the filler was initially bonded to the matrix. Cohesive zone modelling (CZM) was then introduced using the traction-separation law shown in Fig. 6(a).

The three modes of failure in CZM are usually referred to as opening mode I (normal tension mode), mode II (shear mode), or mode III (out of plane shear mode) (Camanho and Davila 2002; Magnusson and Ostlund 2013). The traction *versus* separation law used to model the cohesive zone is described as,

$$\mathbf{t} = \mathbf{K}\boldsymbol{\delta} = \begin{Bmatrix} t_n \\ t_s \\ t_t \end{Bmatrix} = \begin{bmatrix} K_{nn} & 0 & 0 \\ 0 & K_{ss} & 0 \\ 0 & 0 & K_{tt} \end{bmatrix} \begin{Bmatrix} \delta_n \\ \delta_s \\ \delta_t \end{Bmatrix}. \quad (5)$$

where **t** is the nominal traction stress vector, **K** is the coefficient tensor, and **δ** is the separation vector. The subscripts in Eq. 5, K_{nn}, K_{ss}, and K_{tt}, represent the normal, shear, and tangential coefficients, respectively. Mode I and mode II debonding for a 2-D traction-separation behaviour can be obtained from Eq. 5, which reduces to:

$$\mathbf{t} = \mathbf{K}\boldsymbol{\delta} = \begin{Bmatrix} t_n \\ t_s \end{Bmatrix} = \begin{bmatrix} K_{nn} & 0 \\ 0 & K_{ss} \end{bmatrix} \begin{Bmatrix} \delta_n \\ \delta_s \end{Bmatrix}. \quad (6)$$

The traction *versus* separation law for each mode of failure can be separated into two regions (Abaqus 2009; Camanho and Davila 2002), as shown in Fig. 6(a). In the first region, the traction-separation graph is linear elastic and is described using Eq. 6. In the second region, which occurs at a critical normal stress, t_n^o (or shear stress, t_s^o or tangential stress, t_t^o), damage/debonding is initiated. Debonding is activated in terms of a maximum stress criterion expressed as:

$$\max\left\{\frac{\langle t_n \rangle}{t_n^0}, \frac{t_s}{t_s^0}, \frac{t_t}{t_t^0}\right\} = 1 \quad (7)$$

where the symbol $\langle t_n \rangle$ represents the Macaulay bracket, defined as $\langle t_n \rangle = \frac{1}{2}\left(|t_n| + t_n\right)$, implying that debonding is not initiated in compression. Progressive debonding in the interface occurs until complete failure/debonding.

The damage/debonding evolution law describes the rate at which the cohesive stiffness is degraded after the damage/debonding initiation criterion is reached. For 2-D traction separation behaviour, the energy that is dissipated as a result of the debonding process (*i.e.*, the cohesive energy (G_c)), is equal to the area under the traction-separation curve in Fig. 6(a).

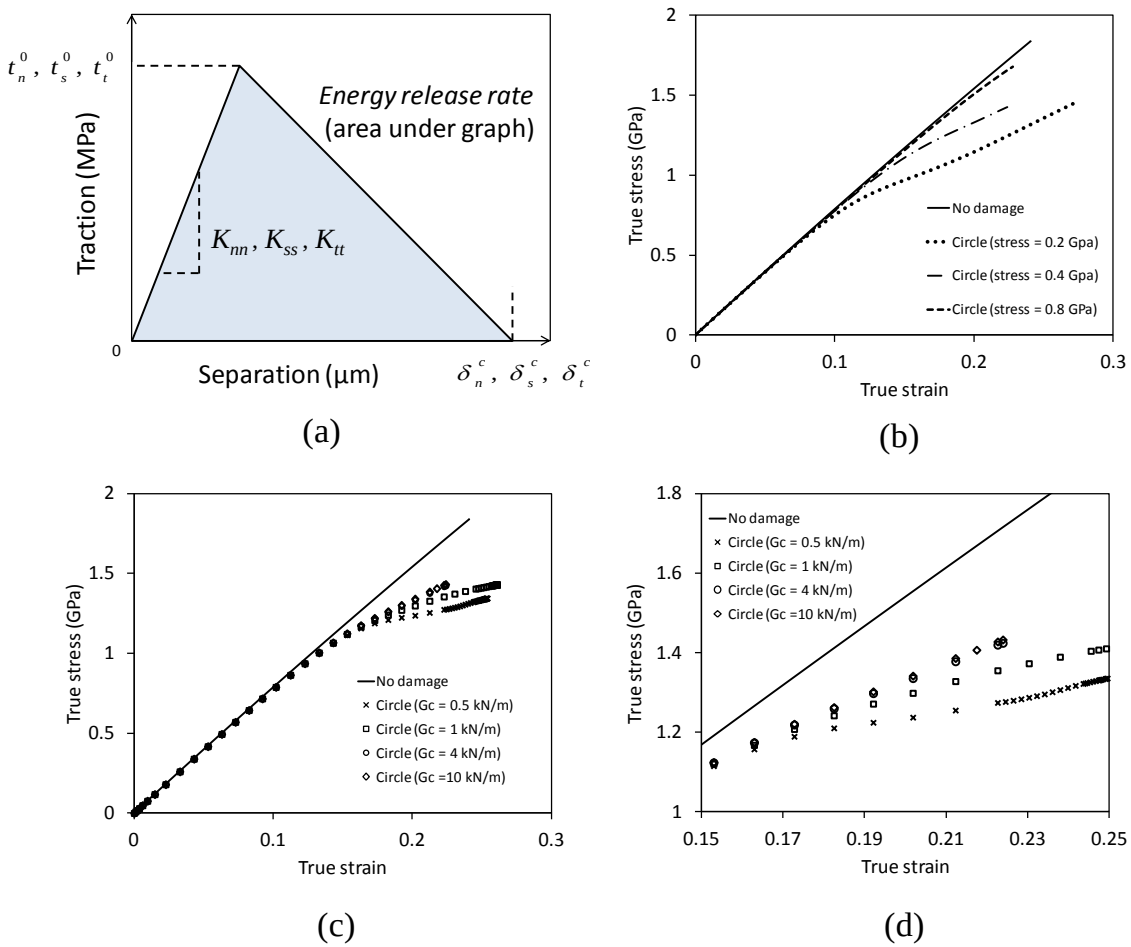

Fig. 6. (a) Traction *versus* separation of the cohesive damage/debonding model under mode I, mode II, or mode III. Parametric study of CZM under uniaxial tension for (b) critical stress, t_n^0, and (c) different G_c; (d) shows close-up results using different G_c.

To investigate the effect of cohesive damage/debonding parameters on the stress-strain curve of OPEFB, a parametric study of cohesive zone modelling (CZM) was performed. The cohesive debonding parameters were first set as follows: $K_{nn} = K_{ss} = 1 \times 10^8$ GPa/m, $G_c = 4$ kN/m (kJ/m^2), and the critical normal stress was $t_n^0 = 0.4$ GPa. Two of these were then kept constant while varying the third in a parametric study. K_{nm} and K_{ss} were set to be high to prevent interpenetration of the element faces and to prevent artificial compliance from being introduced into the model (Song *et al.* 2008). The critical normal stress value was estimated from the uniaxial tension stress-strain results shown in Figs. 4 and 5. The cohesive energy, $G_c = 4$ kN/m (kJ/m^2), was set by setting the critical separation, δ_n^c (see Fig. 6(a)) at twice the size of the filler (20 μm).

The parametric study results are shown in Fig. 6(b) to Fig. 6(d). Only the results with the circular filler are shown because the simulations of models with spikes were terminated prematurely before any effect of CZM could be observed. It can be seen in Fig. 6(b) that once the critical stress was activated, the stress-strain curve deviated from the no-damage (no-debonding) model. A close-up of the results in Fig. 6(c) is shown in Fig. 6(d) for the strain range of 0.15 to 0.25. The results suggested that the value of cohesive energy should be between 0.5 kN/m and 4 kN/m. Values lower than 0.5 kN/m

are not preferred because the critical separation for 0.5 kN/m is too small (2.5 μm). Likewise, values larger than 4 kN/m are not preferred, as the results at higher energy values are similar (*e.g.*, the results using 4 kN/m and 10 kN/m in Fig. 6(d)).

The minimum cohesive energy value (0.5 kN/m) suggests a strong adhesion between silica bodies and OPEFB fibres. This is comparable to different heterogeneous materials, such as epoxy-glass material (0.4 kN/m; Pan and Pelegri (2011)). The next section will therefore provide some explanation of the silica bodies and OPEFB fibre sub-components (*e.g.*, lignocelluloses) to provide some understanding of the interface between silica bodies and OPEFB fibres.

Composition, Occurrence, and Lignocellulosic-associated Silica Bodies

Silica occurs in nature primarily in the form of silicon dioxide, which consists of silicon and oxygen. Usually, this element will be taken up in the form of silicic acid, a water-soluble and uncharged monomeric molecule that is commonly transported through xylem sap tissue (Ma and Yamaji 2006; Prychid *et al.* 2003). With the aid of transpiration, precipitation, and polymerisation, the accumulated silicic acids will then be concentrated, resulting in the formation of colloidal silicic acid and silica gel, where finally intra and extracellular silica bodies will be formed (Neethirajan *et al.* 2009). As mentioned by Prychid *et al.* (2003), silica bodies are also known as opaline phytoliths and are most commonly found in the epidermis or in the sheath cells of vascular bundles. The number of silica bodies per cell varies, and the location is highly dependent on the location of the cells and the plant species. Silica bodies may develop into many kinds of morphologies; however, the most common morphologies formed in monocotyledons are "druse-like" spherical, spherical rugose, or spherical-spinulose (Prychid *et al.* 2003). As observed by Lins *et al.* (2002), silica bodies are embedded, rough, spherical masses. They were described as spherical, globular subunits with sharp spikes on the outer layer of the subunits. The silica bodies were embedded in their own craters, located in extracellular cavities within the hypodermal layer of cells. The diameters of the silica bodies were also measured and fell within the range of 6 to 10 μm, with a mean of 7.8 μm. However, the diameters were slightly different in the current findings; they ranged between 15 and 23 μm. This is due to the diversity of silica bodies in terms of morphology, size, location, and composition, which vary with species and genera (Prychid *et al.* 2003).

The association of the silica bodies and fibre matrix of the OPEFB has not yet been fully elucidated. Prychid *et al.* (2003) reported that the silica bodies infill the cell lumens and bind to cellulose in the cell walls. This will form a silico-cellulose membrane, where the cell wall is silicified and the strength will be increased. It has been claimed that the silica bodies may be located within the cell wall or between the cellulose wall and plasma membrane. This suggests that silica bodies could act as an initial protector of the cell wall components. Therefore, the absence of silica bodies may increase the cellulosic accessibility to the enzymes, resulting in good digestibility and hydrolysis performance. This is in agreement with Yunus *et al.* (2010), where the authors claim that the silica bodies can impede penetration into a lignocellulosic matrix. Silica bodies have also been suspected to act as a barrier to enzymatic hydrolysis, as they hinder enzyme penetration into the inner layer of the OPEFB (Bahrin *et al.* 2012; Hamzah *et al.* 2011). A study by Najafpour *et al.* (2007) also confirmed that the removal of silica bodies from OPEFB fibre could expose the active sites of cellulose and thus increase sugar yield. In a work by Isroi *et al.* (2012), fungal communities were observed to be concentrated on the empty silica body sites. From this phenomenon, it is likely that the removal of silica bodies can

be a key point in exposing the cellulose or hemicellulose materials because bacterial and fungal colonisation actions are very substrate-specific. Removal of silica bodies may be performed using a number of methods, such as physical treatments (Law *et al.* 2007), physico-chemical treatments (Bahrin *et al.* 2012), and biological treatments (Isroi *et al.* 2012), where the last two methods have shown better results when performed together. There is a great need to remove silica bodies effectively for lignocellulosic materials from OPEFB to be used as various bioresources and value-added bioproducts. Hopefully, the method of obtaining critical stress and cohesive energy for silica body removal from OPEFB in this work will become a starting point for studying this important, yet not fully understood, mechanism.

CONCLUSIONS

1. An investigation of the microstructure of silica bodies on OPEFB fibre surfaces using scanning electron microscopy (SEM) was performed in this work. The information from image analysis was used in finite element modelling of OPEFB by treating OPEFB as a heterogeneous material.
2. The parameters investigated included the effect of silica body geometry, possible anisotropy/orthotropy, and debonding between the interface of the silica body and OPEFB fibres.
3. The results of the circular model with occurrence of spikes showed agreement with those of a perfectly circular filler. The cohesive zone modelling results, on the other hand, showed deviation of the stress-strain curve from the no-damage (no-debonding) model once the critical debond stress was activated.

ACKNOWLEDGEMENTS

Universiti Putra Malaysia Grant Scheme 2013 (GP-IPM/2013/9405300) and Knowledge Transfer Programme (KTP 6228118) grants sponsored by the Ministry of Higher Education (MoHE) of Malaysia and Universiti Putra Malaysia greatly contributed to the present research.

REFERENCES CITED

Abaqus (2009). *User Manual ver. 6.9*, Hibbitt Karlsson and Sorensen, Providence, RI.

Bahrin, E. K., Baharuddin, A. S., Ibrahim, M. F., Razak, M. N. A., Sulaiman, A., Abd-Aziz, S., Hassan, M. A., Shirai, Y., and Nishida, H. (2012). "Physicochemical property changes and enzymatic hydrolysis enhancement of oil palm empty fruit bunches treated with superheated steam," *BioResources* 7(2), 1784-1801.

Burgert, I. (2006). "Exploring the micromechanical design of plant cell walls," *Am. J. Bot.* 93(10), 1391-1401.

Burgert, I., and Dunlop, J. W. C. (2011). "Micromechanics of cell walls," *Mech. Integ. Plant Cells and Plants* 9, 27-52.

Camanho, P. P., and Davila, C. G. (2002). "Mixed-mode decohesion finite elements for the simulation of delamination in composite materials," *NASA Technical Report*, NASA/TM-2002-211737, 1-37.

Currie, H. A., and Perry, C. C. (2007). "Silica in plants: Biological, biochemical and chemical studies," *Ann. Bot.* 100(7), 1383-1389.

d'Almeida, J. R. M., Aquino, R. C. M. P., and Monteiro, S. N. (2006). "Tensile mechanical properties, morphological aspects and chemical characterization of piassava (*Attalea funifera*) fibers," *Compos. Part A: Appl. Sci. Manuf.* 37(9), 1473-1479.

Fang, J., and Ma, X. (2006). "In vitro simulation studied on silica deposition induced by lignin from rice," *J. Zhejiang Univ. Sci. B* 7(4), 267-271.

Gunawan, F. E., Homma, H., Brodjonegoro, S. S., Hudin, A. B., and Zainuddin, A. (2009). "Mechanical properties of oil palm empty fruit bunch fiber," *J. Solid Mech. Mater. Eng.* 3(7), 943-951.

Hamzah, F., Idris, A., and Shuan, T. K. (2011). "Preliminary study on enzymatic hydrolysis of treated oil palm (*Elaeis*) empty fruit bunches fibre (EFB) by using combination of cellulase and β 1-4 glucosidase," *Biomass Bioenergy* 35(3), 1055-1059.

Hayot, C. M., Farousech, E., Goel, A., Avramova, Z., and Turner, J. A. (2012). "Viscoelastic properties of cell walls of single living plant cells determined by dynamic nanoindentation," *J. Exp. Bot.* 63(7), 2525-2540.

Hubbe, M. A., and Heitmann, J. A. (2007). "Review of factors affecting the release of water from cellulose fibers during paper manufacture," *BioResources* 2(3), 500-533.

Isroi, Ishola, M. M., Millati, R., Syamsiah, S., Cahyanto, M. N., Niklasson, C., and Taherzadeh, M. J. (2012). "Structural changes of oil palm empty fruit bunch (OPEB) after fungal and phosphoric acid pretreatment," *Molecules* 17(12), 14995-15012.

Law, K. N., Daud, W. R. W., and Ghazali, A. (2007). "Morphology and chemical nature of fiber strands of oil palm empty-fruit-bunch (OPEFB)," *BioResources* 2(3), 351-362.

Lins, U., Barros, C. F., da Cunha, M., and Costa-Miguens, E. (2002). "Structure, morphology and composition of silicon biocomposites in the palm tree *Syagrus coronate* (Mart.) Becc," *Protoplasma* 220(1-2), 89-96.

Ma, J. F., and Yamaji, N. (2006). "Silicon uptake and accumulation in higher plants," *Trends Plant Sci.* 11(8), 392-397.

Magnusson, M. S., and Ostlund, S. (2013). "Numerical evaluation of interfibre joint strength measurements in terms of three-dimensional resultant forces and moments," *Cellulose* 20(4), 1691-1710.

Martin-Sampedro, R., Rodriguez, A., Ferrer, A., García-Fuentevilla, L. L., and Eugenio, M. E. (2012). "Biobleaching of pulp from oil palm empty fruit bunches with laccase and xylanase," *Bioresour. Technol.* 110, 371-378.

Meddad, A., and Fisa, B. (1997). "A model for filler-matrix debonding in glass-bead-filled viscoelastic polymers," *J. Appl. Polym. Sci.* 65(10), 2013-2024.

Mishnaevsky, L. (2007). *Computational Mesomechanics of Composites: Numerical Analysis of the Effect of Microstructures of Composites on Their Strength and Damage Resistance*, John Wiley and Sons, Chichester.

Najafpour, G., Ideris, A., Salmanpour, S., and Norouzi, M. (2007). "Acid hydrolysis of pretreated palm oil lignocellulosic wastes," *IJE Transactions B: Applications* 20(2), 147-156.

Nascimento, D. C. O., Ferreira, A. S., Monteiro, S. N., Aquino, R. C. M. P., and Kestur, S. G. (2012). "Studies on the characterization of piassava fibers and their epoxy composites," *Compos. Part A: App. Sci. Manuf.* 43(3), 353-362.

Neethirajan, S., Gordon, R., and Wang, L. (2009). "Potentials of silica bodies (phytoliths) for nanotechnology," *Trends Biotechnol.* 27(8), 461-467.

Nordin, N. I. A., Ariffin, H., Andou, Y., Hassan, M. A., Shirai, Y., Nishida, H., Yunus, W. M. Z. W., Karuppuchamy, S., and Ibrahim, N. A. (2013). "Modification of oil palm mesocarp fiber characteristics using superheated steam treatment," *Molecules* 18, 9132-9146.

Pan, Y., and Pelegri, A. A. (2011). "Progressive damage analysis of random chopped fiber composite using finite elements," *J. Eng. Mater. Tech.* 133(1), 011018.

Prychid, C. J., Rudall, P. J., and Gregory, M. (2003). "Systematics and biology of silica bodies in monocotyledons," *Bot. Rev.* 69(4), 377-440.

Qing, H., and Mishnaevsky, L. (2009). "3D hierarchical computational model of wood as a cellular material with fibril reinforced, heterogeneous multiple layers," *Mech. Mater.* 41(9), 1034-1049.

Qing, H., and Mishnaevsky, L. (2011). "A 3D multilevel model of damage and strength of wood: Analysis of microstructural effects," *Mech. Mater.* 43(9), 487-495.

Rasband, W. S. (2012). *ImageJ*, U.S. National Institutes of Health, Bethesda, Maryland.

Somerville, C., Bauer, A., Brininstool, G., Facette, M., Hamann, T., Milne, J., Osborne, E., Paredez, A., Persson, S., Raab, T., Vorwerk, S., and Youngs, H. (2004). "Towards a systems approach to understanding plant cell walls," *Science* 306(5705), 2206-2211.

Song, K., Davila, C. G., and Rose, C. A. (2008). "Guidelines and parameter selection for the simulation of progressive delamination," *ABAQUS User's Conference*, Newport, RI, Hibbit Karlsson and Sorensen, pp. 1-15.

Underwood, E. E. (1970). *Quantitative Stereology*, Addison-Wesley, New York.

Yunus, R., Salleh, S. F., Abdullah, N., and Awg-Biak, D. R. (2010). "Effect of ultrasonic pre-treatment on low temperature acid hydrolysis of oil palm empty fruit bunch," *Bioresour. Technol.* 101(24), 9792-9796.

Yusoff, M. Z. M., Salit, M. S., and Ismail, N. (2009). "Tensile properties of single oil palm empty fruit bunch (OPEFB) fibre," *Sains Malays.* 38(4), 525-529.

Article submitted: October 2, 2013; Peer review completed: December 5, 2013; Revised version received and accepted: December 16, 2013; Published: December 20, 2013.